Published in final edited form as:
Contrast Media Mol Imaging. 2011 ; 6(6): 474–481. doi:10.1002/cmmi.447.

ß-cell Subcellular Localization of Glucose Stimulated Mn Uptake By X-ray Fluorescence Microscopy: Implications for Pancreatic MRI

Lara Leoni[1], **Anita Dhyani**[1], **Patrick La Riviere**[1], **Stefan Vogt**[2], **Barry Lai**[2], and **B.B. Roman**[*,1,3]

[1]Department of Radiology, Committee on Medical Physics, University of Chicago, Chicago, IL, USA

[2]X-ray Science Division, Argonne National Laboratory, 9700 South Cass Avenue, Argonne, IL, USA

[3]Committee on Metabolism and Nutrition, University of Chicago, Chicago, IL, USA

Abstract

Manganese (Mn) is a calcium (Ca) analog that has long been used as a magnetic resonance imaging (MRI) contrast agent for investigating cardiac tissue functionality, for brain mapping and for neuronal tract tracing studies. Recently, we have extended its use to investigate pancreatic β-cells and showed that, in the presence of $MnCl_2$, glucose activated pancreatic islets yield significant signal enhancement in T_1-weigheted MR images. In this study, we exploited for the first time the unique capabilities of X-ray fluorescence microscopy (XFM) to both visualize and quantify the metal in pancreatic β-cells at cellular and sub-cellular levels. MIN-6 insulinoma cells grown in standard tissue culture conditions had only a trace amount of Mn, $1.14 \pm 0.03 \times 10^{-11}$ μg/μm^2, homogenously distributed across the cell. Exposure to 2mM glucose and 50 μM $MnCl_2$ for 20 minutes resulted in non-glucose dependent Mn uptake and the overall cell concentration increased to $8.99 \pm 2.69 \times 10^{-11}$ μg/μm^2. When cells were activated by incubation in 16mM glucose in the presence of 50 μM $MnCl_2$, a significant increase in cytoplasmic Mn was measured reaching $2.57 \pm 1.34 \times 10^{-10}$ μg/μm^2. A further rise in intracellular concentration was measured following KCl induced depolarization, with concentrations totaling $1.25 \pm 0.33 \times 10^{-9}$ and $4.02 \pm 0.71 \times 10^{-10}$ μg/μm^2 in the cytoplasm and nuclei respectively. In both activated conditions Mn was prevalent in the cytoplasm and localized primarily in a perinuclear region, possibly corresponding to the Golgi apparatus and involving the secretory pathway. These data are consistent with our previous MRI findings confirming that Mn can be used as a functional imaging reporter of pancreatic β-cell activation and also provide a basis for understanding how subcellular localization of Mn will impact MRI contrast

Keywords

manganese; sub-cellular localization; pancreatic β-cells function; X-ray fluorescence microscopy; MRI

[*]Corresponding Author Brian B. Roman, Ph.D., Assistant Professor, Department of Radiology, MC2026, University of Chicago, 5841 S. Maryland Ave., Chicago, IL, USA 60637, Phone: 773-702-6906, Fax: 773-702-1161, broman@uchicago.edu.

Introduction

Manganese (Mn) has long been used in biological applications as a calcium (Ca) analog in fluorescence light microscopy and increasingly as a positive contrast agent in T_1-weighted MRI where it has been used for brain mapping [1], neuronal tract tracing [2], and cardiac functional studies [3]. Manganese-enhanced MRI (MEMRI) exploits the biological and biophysical properties of Mn to identify anatomical structures and their Ca-related activation in excitable tissues and organs due to its ability to readily enter cells through voltage-gated calcium channels [4]. Recently MEMRI has found new and exciting applications, such as the characterization of pancreatic beta-cell activation, which are contributing to the renewed and fast-growing interest in Mn [5, 6]. Mn induces changes in the longitudinal T_1 relaxation rate of water that are used to quantify cell or tissue function. However the sub-cellular basis of these changes is poorly understood due to the experimental complexity involved in assessing sub-cellular Mn accumulation and distribution. Although T_1 changes can be measured, their significance depends not on the overall Mn tissue concentration but rather on the effective relaxivity. This is determined by the distribution and the chemical and biophysical state of the paramagnetic ions, i.e. whether the ions are free, bound, chelated, or complexed with macromolecules, as these parameters determine the access of protons to the ion and ultimately the magnitude of changes in T_1 relaxation times.

We have previously shown that MEMRI can be used to assess pancreatic beta cell function [5-9] both in vitro and in vivo using rodent models. Here we are interested in understanding the molecular basis of Mn MRI enhancement by understanding how β-cells accumulate and metabolize Mn in the resting state and in response to glucose stimulation when exposed acutely to non-toxic Mn concentrations. X-ray fluorescence microscopy (XFM) is a powerful technique that allows acquisition and analysis of quantitative elemental maps of trace metals with submicron resolution in cell and tissue samples [10-12]. We were able to visualize and quantify the cellular and subcellular topography of Mn and found that total Mn levels in MIN-6 β-cells increased significantly following glucose stimulation and KCl induced depolarization.

To the best of our knowledge few studies so far have linked MR signal enhancement to tissue or cellular Mn concentration, with almost all of them focusing on the brain [13-17]. Interestingly, in olfactory bulbs, the highest Mn accumulation was found to be in the microsomal fraction [17], while other brain cell types showed a cell-type specific uptake, with nuclei having the highest Mn concentration [18, 19]. As in olfactory bulb neurons,, we found that mouse insulinoma cells preferentially sequestered Mn in the cytoplasm. These findings provide a solid foundation for using MEMRI in functional studies of pancreatic islets and further validate our previous findings.

Materials and Methods

Cells

MIN-6 cells were cultured in DMEM Glutamax™ (Invitrogen Life Technology, Carlsbad, CA) supplemented with 10% Fetal Bovine Serum (Mediatech, Manassas, VA) and 1% Penicillin-Streptomycin (Mediatech, Manassas, VA).

X-ray Fluorescence Microscopy Samples

Silicon nitride windows (Silson Ltd., Northampton, UK) with membrane size 2.0 mm × 2.0 mm and 500 nm membrane thickness were rinsed with complete DMEM media and placed in 6-well plates. Approximately 10^4 MIN-6 cells were seeded on each window and incubated in supplemented DMEM media for 48 hours prior to being treated. On the day of treatment, all windows were rinsed in phosphate buffer solution (PBS) three times and then

incubated for 20 minutes in Krebs-Ringer buffer solution (KRB) supplemented with 2mM glucose. Samples were then incubated for an additional 20 minutes in the following conditions: a) KRB supplemented with 2 mM glucose and 50 μM $MnCl_2$; b) KRB supplemented with 16 mM glucose and 50 μM $MnCl_2$; c) KRB supplemented with 16 mM glucose, 50 μM $MnCl_2$ and 30 mM KCl. MIN-6 cells cultured for 48 hours on the silicon nitride windows in standard culture conditions were used as control (d). All samples were rinsed three times in PBS and fixed in 4% paraformaldehyde in PBS for 20 minutes followed by several washes in 20 mM Pipes/200 mM sucrose pH 7.2 and then were air dried. The samples analyzed were obtained from two separate experiments.

X-ray Fluorescence Microscopy and Analysis

Samples were imaged at the 2-IDD beamline station at the Advanced Photon Source at Argonne National Laboratory (Argonne, IL) using 10-KeV incident energy X-rays. The samples were first observed in brightfield mode on a light microscope (DMXRE Leica Mycrosystems, Wetzlar, Germany) in order to identify regions of interest (ROIs). The X and Y coordinates of the ROIs relative to the four window corners were measured and served as reference to precisely locate the ROIs once samples were mounted on the x-ray fluorescence probe. Undulator-generated x-rays were monochromatized with a double crystal (Si <111>) monochromator and focused using Fresnel zone plate optics (X-radia, Concord, CA). Selected ROIs were raster-scanned in steps of 400×400 nm, 300×300 nm or 200×200 nm and fluorescence spectra were collected for each pixel for 1-sec dwell time by using an energy dispersive silicon drift detector (SII NanoTechnology, Northridge, CA). Quantitation and image processing were performed with MAPS software [20]. Standardization to convert the fluorescence signal to a two-dimensional concentration in $\mu g/cm^2$ was achieved by fitting spectra against signal derived from thin-film standards NBS-1832 and NBS-1833 (National Bureau of Standards, Gaithersburg, MD). Each image represents a two-dimensional projection of the cells.

ROIs were drawn only around well identifiable single cells. Within each cell both the nuclear and the cytoplasmatic compartments were analyzed separately. For the control group 8 single cells were analyzed; for the 2mM glucose and Mn condition 11 were analyzed; for the 16mM glucose and Mn condition 9 were analyzed; and for the 30mM KCl and Mn condition 7 were analyzed. Considering that only a very limited number of cells can be imaged with XFM during each scan, these sample numbers are well within the meaningful range [11, 21]. All data are presented as mean ± SD. Statistical significance was evaluated using a single-factor ANOVA test. A probability value of <0.05 was considered to be significant.

Scanning Electron Microscopy

MIN-6 cells grown in T25 tissue culture flasks were exposed to Mn and glucose according to the patterns (a-d) described above. After rinsing three times in PBS, cells were fixed in 2% glutaraldehyde and 4% paraformaldehyde in 0.1M sodium cacodylate buffer, scraped off the flasks and pelleted. Samples were post-fixed for 60 minutes in 1% osmium tetroxide in the same buffer and stained with 1% uranyl acetate in maleate buffer. All samples were progressively dehydrated in graded ethanol and propylene oxide, and embedded in Spurr resin. Ninety nanometer sections were examined under 300KV at FEI Tecnai F30. All chemicals were from Ted Pella Inc., Redding, CA.

Fluorescence Cell Labeling

MIN-6 cells were grown on coverslips for 48 hours and were fixed in 4% formalin PBS buffer for 15 minutes at room temperature. They were permeabilized for 10 minutes with PBT (0.1% Triton X-100 in PBS). The Golgi apparatus was labeled by incubating for 20

minutes in a PBS solution of a 5 μg/ml green-fluorescent Alexa Fluor® 488 conjugate of HPA lectin (Invitrogen, Carlsbad, CA). Nuclei were counterstained with DAPI (Invitrogen, Carlsbad, CA).

RESULTS

Intracellular Manganese Uptake by MIN-6 Insulinoma β-cells

In order to understand how intracellular Mn contributes to MRI signal enhancement in pancreatic β–cells specifically and to confirm its validity as a functional reporter, clusters of fixed MIN-6 cells previously exposed to 50 μM $MnCl_2$ in resting or insulin secreting conditions were analyzed using XFM, as were control cells not exposed to Mn. Cells in the control group (group d) had only trace amounts of Mn quantified at $1.14\pm0.03 \times 10^{-11}$ μg/μm^2 (Figure 1). This was expected as the media formulation does not include Mn among the ingredients. A statistically significant increase in intracellular Mn accumulation was found in MIN-6 cells incubated with 50 μM $MnCl_2$ at the resting (2 mM glucose) condition (group a). The Mn concentration was found to be $8.99 \pm 2.69 \times 10^{-11}$ μg/μm^2 or an almost 8 fold increase over the control group ($p< 0.01$) reflecting non-specific crossing of the plasma membrane via facilitated diffusion. Although no data is available for pancreatic β-cells, Schramm and Brandt found that in isolated rat hepatocytes facilitated diffusion had a K_m for Mn^{2+} of 1.2 μM and a V_{max} equal to 54 nmol/min/g cells [22]. Other studies on rat and chick glial cells found the apparent K_m to be 0.3 μM and 18 μM respectively [23]. It is therefore plausible to regard plasma membrane facilitated transport of Mn as responsible for the accumulation of the metal measured at 2mM glucose.

During glucose induced active transport (group b) intracellular Mn concentration reached $2.02 \pm 0.49 \times 10^{-10}$ μg/μm^2 or a 2.2 fold increase over the 2mM glucose group ($p<0.001$). Additional depolarization caused by the addition of 30mM KCl in the extracellular media (group c) resulted in a further significant jump in intracellular Mn to $7.42 \pm 2.02 \times 10^{-10}$ μg/μm^2 ($p<0.001$), or about 3.5 and 8 fold over the 16mM glucose and 2mM glucose samples respectively.

Spatial Distribution and Localization of Intracellular Manganese

The subcellular localization of Mn is often overlooked but is quite relevant to understanding the Mn-enhanced MRI signal. Over the incubation time we considered, a clear trend was observed in MIN-6 β-cells where Mn went from a rather uniform distribution across the whole cell in the control (group d) and low glucose (group a) samples to an increasingly cytoplasmic one in both stimulated conditions (groups b and c) with over 70% of total Mn ending up in the cytoplasm. Consequently, the effective Mn concentrations in nuclei and cytoplasm vary with non-glucose dependent Mn uptake, $7.80\pm3.31 \times 10^{-11}$ μg/μm^2 and $1.04\pm0.34 \times 10^{-10}$ μg/μm^2 respectively, although not in a statistically significant manner as shown in Figure 2. In activated cells, the sharp shift to cytoplasmic accumulation brings the final concentration to $2.57\pm1.34 \times 10^{-10}$ μg/μm^2 at 16mM glucose and $1.25\pm 0.33 \times 10^{-9}$ μg/μm^2 following KCl depolarization, corresponding to approximately 2.5 and 10 fold increase over the baseline ($p<0.01$). Pseudocolored XFM micrographs shown in Figure 3 illustrate specific localization of Mn. The strong phosphorus signal coming from the nucleic acids was used to identify the nuclei as represented by the intense red pseudocoloring shown in the left panel. The middle panel clearly shows Mn enriched areas that were pseudocolored in green, with a characteristic granular appearance similar to what was reported by Morello and others [18]. Staining of the samples following X-ray exposure could not be performed due to radiation damage. Instead, SEM graphs of different groups of MIN-6 cells representing all experimental conditions were acquired to correlate Mn with intracellular structures. No significant difference in cytoplasmic organization was found among the four groups. A

representative scan of a 16 mM glucose, 30 mM KCl and 50 μM $MnCl_2$ cell (group c) is shown in Figure 4a. The nucleus is clearly visible in the left region of the cell, with mitochondria dispersed homogeneously in the cytoplasm (white arrows). Several small black dots which correspond to insulin granules are easily identifiable but no definitive correlation was made between cellular structures and the Mn rich perinuclear regions highlighted in Figure 3. SEM scans capture only a thin section of the cell, therefore not all structures are observed. Fluorescent staining is, like XFM, a 2D representation of the whole 3D structure, and identified the Golgi apparatus as intense green fluorescence areas around the DAPI stained nuclei (Figure 4b). Although a correlation can be made, an association could not be directly established.

Discussion

The goal of this study was to better understand the mechanisms of MRI enhancement specifically in β-cells due to Mn intracellular accumulation. Understanding how Mn is regulated and handled by different cell types is fundamental in understanding MRI signal enhancement, the physiological implications and in optimizing the contrast agent dose. MEMRI has been used extensively to study excitable cells, but only recently has it been used as a reporter of pancreatic β-cell function [5-7, 24]. Our previous in vitro studies on both rodent and human isolated islets have shown a significant increase in Mn-induced MRI signal following glucose stimulation [5, 6]. In vivo data on rodent endogenous pancreas has also confirmed the validity of this technique [7, 24], although the interpretation of Mn signal enhancement is complicated by the anatomy and morphology of the pancreas and by the complex cellular interactions of Mn. The pancreas is known to be a preferential site of Mn accumulation following in-vivo systemic administration of $MnCl_2$ [25-27]. Nonetheless, only a handful of studies so far have investigated distribution of the element in the organ with no distinction between exocrine and endocrine components. Mn was found to accumulate primarily in lysosomes where it is bound to pro-carboxypeptidase B, a zymogen found in the exocrine portion of the pancreas [28, 29]. Two studies on isolated rodent pancreatic islets used Mn to study Ca handling in β-cells and found a significant Mn uptake following glucose stimulation in all fractions, except for microsomes, with the mitochondrial fraction having the highest percentage increase [30, 31].

Lacking a suitable staining technique for Mn, most studies only assess Mn amounts in cells and tissues using atomic absorption spectroscopy [15, 30-33], inductively-coupled plasma-mass spectroscopy (ICP-MS) [16, 28], or by means of radioactivity using ^{54}Mn [19, 22, 34]. All techniques are fairly accurate and have appropriate detection limits. Conversely they provide only an average concentration of Mn present in the homogenate or in the different cellular fractions that are isolated following complex protocols that risk washing out significant amounts of the metal. A nearly 50% loss of soluble endogenous Mn during was reported during processing of brain samples for electron spectroscopy imaging (ESI) and electron-loss spectroscopy (ELS) [18]. Comparing Mn concentrations from this study with preliminary data obtained from samples fixed using plunge freezing followed by vacuum drying, (which do not involve any washing) we found the values for groups a,b, and d to be equivalent (unpublished data). The limited literature available on Mn quantitation via XFM supports our data [21, 35]. Single cell Mn concentration (total content/cell volume) was estimated to be 22 μM for untreated MIN-6 cells in good agreement with similar XFM measurements made on HL-60 cells [21]. Nuclear and cytoplasmic concentrations were still comparable and estimated at 250 μM and 285 μM respectively following Mn uptake in resting conditions. Glucose activation caused an increase in cytoplasmic Mn concentration only to about 590 μM while KCl depolarization induced a similarly large increase in both compartments, with nuclear Mn concentration estimated at 1.90 mM and cytoplasmic at 4.40 mM. This demonstrates the presence of abundant cellular binding sites for Mn and the

ability of cells to sequester metals. Although no toxicity studies were performed for this specific study, based on our previous experience with isolated rodent and human islets [5, 6] and on other toxicity studies [36, 37] toxic effects following Mn uptake can be expected only at intracellular concentrations in the tens of millimolar. Isolated human islets activated with 16mM glucose and 50 μM $MnCl_2$ had normal insulin secretion and viability [5]. However, because of diffusion limitations and different calcium channel compositions, it appears that human islets take up less Mn than rodent β-cells. Still, the MR signal enhancement obtained with human tissue was remarkable. The increase in signal to noise ratio (SNR) in T_1 weighted images was 15% following treatment with 50 μM $MnCl_2$ in low glucose and jumped to 46% following glucose stimulation.

We were not able to precisely identify sub-nuclear structures but binding of Mn to nucleic acids has been very well documented. In duplex DNA structures Mn has high affinity and directly coordinates to phosphate oxygen atoms with most of the binding involving a water molecule [38, 39]. Additional binding sites identified involve direct interaction of the metal ions with N_7 of the guanine ring and an interaction with the carbonyl group of cytosine[40]. In the cytoplasm of hepatocytes, brain and cardiac tissues, Mn has been shown to partition between the cytosolic compartment, where is tightly bound to macromlecules, and organelles [18, 22, 37]. Using SEM graphs and fluorescently stained MIN-6 cells as a reference, we can reasonably assume that insulin granules do not play a significant role in binding Mn.

Mitochondria play a fundamental role in Mn regulation in excitable cells [41, 42] and we were surprised not to find discernible regions of high Mn concentrations that could be related to these organelles. This could be due in part to the difficulty in identifying mitochondria based on metal content because of their elongated shape and size ranging within few microns. However, within the overall scheme of Ca, and therefore by association Mn, mitochondrial stores do not appear to be significant in volume or concentration when compared to the ER [43]. Specifically, MIN-6 cells incubated in high glucose and KCl were shown to have a significant increase in cytoplasmic ATP consumption which was linked mainly to Ca pumping into the ER by sarco(endo)plasmic reticulum Ca-ATPase (SERCA) [44]. The ER, the Golgi complex and associated secretory vesicles which make up the secretory pathway, have a high luminal Ca concentration ranging between 0.1 to 2 mM required for proper protein synthesis and processing [45]. These intracellular stores contribute to the regulation of cytosolic Ca and signaling and typically contain calcium-binding proteins. The secretory pathway also requires sufficient Mn for correct glycosilation of proteins. Therefore the accumulation of Mn in the Golgi apparatus also provides a regulatory pathway that helps avoid excessive cytosolic concentrations mostly by means of the Golgi associated secretory-pathway Ca-transport ATPases (SPCAs) [45]. While SERCAs have low Mn affinity, among the known SPCAs, SPCA1 competitively transports Ca and Mn with equally high affinity [45, 46] and was found to be expressed in subcellular fractions of rat and mouse β-cells. In MIN-6 cells specifically, it was found in microsomal and dense-core secretory vescicles, suggesting its association with the ER, the Golgi apparatus and the distal part of the secretory pathway [47]. This is supported by similar findings in rodent olfactory bulbs which were found to have significant Mn increase only in the microsomal fraction [17].

Such partition of intracellular Mn could explain the biphasic nature of its efflux from isolated mouse islets [30], with the portion bound to proteins in the cytoplasm and to nuclei acids being released promptly following withdraw of the metal from the extracellular environment, while the Mn sequestered in the different organelles would contribute to the slow release phase.

Based on our data, in pancreatic β-cells at basal conditions, it appears reasonable to assume that Mn located in the nucleus and the cytoplasm equally contribute to MRI signal enhancement, with T_1 and T_2 values determined by the reduced molecular tumbling of intracellular water. In-vitro and ex-vivo relaxivity studies at low magnetic fields have reported typical r_1 and r_2 relaxivity values being an order of magnitude higher of those measured for simple $MnCl_2$ solutions [38, 48, 49]. However, Mn treated isolated hepatocytes, which had comparable intracellular Mn concentrations as we measured in MIN-6 cells following uptake in 2mM glucose, had similar r_1 and r_2 as aqueous solutions when analyzed at 7.0 T This was explained by the reduced molecular-correlation-time effects at high fields and the possibility of a portion of intracellular Mn being sequestered and therefore not having access to water [50]. The effect of sequestration and the limited access to water could be more relevant at higher glucose concentrations with a significant share of the metal cations having restricted access to water. This is therefore a contributing factor in the lack of change in R_1 relaxation rates at high Mn concentrations, as seen in mouse myocardium at a dose above 197 nmol/g BW, despite increase in absolute Mn content of the heart [51]. Worth noticing is how in our model, following incubation at 16 mM glucose, the increase in intracellular Mn was solely cytoplasmic and consequently the rise in signal intensity (SI) is primarily due to cytoplasmic interactions only. Ideally, a range of Mn concentrations and multiple time points following Mn uptake should be evaluated as Mn travels through the secretory pathway. It would be interesting to evaluate the effect of SPCA1 and/or SERCA inhibitors on signal enhancement. In order to achieve a comprehensive understanding of the cellular and molecular mechanisms of Mn-dependent MRI enhancement, other parameters, specific for each organelle, will have to be determined at a sub-micron resolution which is not achievable with current MR systems.

As cells are dynamic systems, intracellular Mn distribution and concentration will change quickly and in a different manner depending on the extracellular environment [30, 50]. This is even more relevant when MEMRI is applied to whole organs or in-vivo where the degree of complexity is significantly higher and where the overall SI in not only dependent on Mn intracellular topography, but also on its presence in the extracellular and interstitial space as well as in the blood. When considering the in vivo application of MEMRI to pancreatic islets, the organ anatomy is a further complication. In the pancreas the β-cell rich endocrine tissue is highly dispersed within the acinar exocrine tissue which has high affinity for Mn [26, 28, 29, 52]. In rodents, the acquisition of good high resolution images of the pancreas that allow discernment of the two tissue components are hindered by respiratory motion and by low tissue density. This has led investigators to consider the overall changes in SI of the entire pancreas as an indication of β-cell function [24, 52]. Although glucose stimulation is used to increase Mn specificity towards β-cells, understanding the differences in intracellular Mn handling among the different cell types comprising the pancreas would contribute to tailoring MEMRI protocols and would enhance their sensitivity to β-cell functionality. To this end, studies of exocrine tissue and whole pancreas are needed to complement the results presented in this study. XFM has been used to quantify elemental distribution in different tissues [12, 53], however locating pancreatic islets within organ sections could be problematic due to the organ anatomy, and side by side comparison with histology will be necessary. Considering different time points rather than one, as done here, could also help identifying Mn intracellular metabolic pathways and contrast efficiencies. Nonetheless the data presented here is, to the best of our knowledge, the first validation of the sub-cellular origin of MEMRI as a tool to assess β-cell functionality.

Conclusions

Despite recent advancements, non-invasive imaging of pancreatic β-cell mass and function remains problematic although initial promising results have been obtained in rodents with

MEMRI. As MEMRI finds novel applications, there is the need to better understand the cellular and molecular basis of Mn induced MRI contrast. In this study we were able to clearly visualize and quantify intracellular uptake of Mn in mouse MIN-6 β-cells and clearly link it to glucose activation and depolarization due to the extreme sensitivity and specificity of XFS. These results support the validity of MEMRI as a non-invasive tool to assess and follow the functionality of β-cell endocrine tissue over time. Understanding how Mn is metabolized opens the possibility to use this contrast agent for the characterization of cellular and molecular pathways.

Acknowledgments

National Institute of Health grant R01EB001828 and NIH Beta Cell Biology Consortium U01 DK072473 to BBR supported this work. Use of the APS was supported by the U.S. Department of Energy, Office of Science, Office of Basic Energy Sciences, under Contract No. DE-AC02-06CH11357. We would like to thank Dr. Lydia Finney at the Advance Photon Source, Argonne National Laboratory, for technical assistance with sample preparation and imaging.

References

1. de Sousa PL, de Souza SL, Silva AC, de Souza RE, de Castro RM. Manganese-enhanced magnetic resonance imaging (MEMRI) of rat brain after systemic administration of MnCl2: changes in T1 relaxation times during postnatal development. J Magn Reson Imaging. 2007; 25(1):32–8.10.1002/jmri.20792 [PubMed: 17173304]
2. Pautler RG. In vivo, trans-synaptic tract-tracing utilizing manganese-enhanced magnetic resonance imaging (MEMRI). NMR Biomed. 2004; 17(8):595–601.10.1002/nbm.942 [PubMed: 15761948]
3. Hu TC, Pautler RG, MacGowan GA, Koretsky AP. Manganese-enhanced MRI of mouse heart during changes in inotropy. Magn Reson Med. 2001; 46(5):884–90.10.1002/mrm.1273 [PubMed: 11675639]
4. Dryselius S, Grapengiesser E, Hellman B, Gylfe E. Voltage-dependent entry and generation of slow Ca2+ oscillations in glucose-stimulated pancreatic beta-cells. Am J Physiol. 1999; 276(3 Pt 1):E512–8. [PubMed: 10070018]
5. Leoni L, Serai S, Magin RL, Roman BB. Functional MRI Characterization of Isolated Human Islet Activation. NMR Biomed. 2010; 23:1–9.10.1002/nbm.1542 [PubMed: 20088003]
6. Gimi B, Leoni L, Oberholzer J, Braun M, Avila J, Wang Y, et al. Functional MR microimaging of pancreatic beta-cell activation. Cell Transplant. 2006; 15(2):195–203. [PubMed: 16719054]
7. Haque ME, Vargas P, Markiewicz E, Dhyani A, Leoni L, La Riviere PJ, et al. High Resolution and Multisclice Functional MRI of Pancreatic Beta Cell Activation. Imaging the Pancreatic Beta Cell, 4th Workshop. 2009; 2009:43.
8. Leoni L, Roman BB. MR Imaging of Pancreatic Islets: Tracking Isolation, Transplantation and Function. Curr Pharm Des. 2010
9. Haque, ME.; Xiaobing, F.; Markiewicz, EJ.; Leoni, L.; Roman, BB. In-Vivo Manganese Enhanced Dynamic Magnetic Resonance Imaging (MEDMRI) to Evaluate Progression of Diabetes in Rodent Pancreas. Proceedings of the 17th Annual Meeting of ISMRM; Honolulu, Hawai'i, USA. 2009.
10. Paunesku T, Vogt S, Irving TC, Lai B, Barrea RA, Maser J, et al. Biological applications of X-ray microprobes. Int J Radiat Biol. 2009; 85(8):710–3.10.1080/09553000903009514 [PubMed: 19637082]
11. Finney L, Mandava S, Ursos L, Zhang W, Rodi D, Vogt S, et al. X-ray fluorescence microscopy reveals large-scale relocalization and extracellular translocation of cellular copper during angiogenesis. Proc Natl Acad Sci U S A. 2007; 104(7):2247–52.10.1073/pnas.0607238104 [PubMed: 17283338]
12. Kehr S, Malinouski M, Finney L, Vogt S, Labunskyy VM, Kasaikina MV, et al. X-ray fluorescence microscopy reveals the role of selenium in spermatogenesis. J Mol Biol. 2009; 389(5):808–18.10.1016/j.jmb.2009.04.024 [PubMed: 19379757]

13. Chaki H, Furuta S, Matsuda A, Yamauchi K, Yamamoto K, Kokuba Y, et al. Magnetic resonance image and blood manganese concentration as indices for manganese content in the brain of rats. Biol Trace Elem Res. 2000; 74(3):245–57.10.1385/BTER:74:3:245 [PubMed: 11055811]
14. Lee JH, Silva AC, Merkle H, Koretsky AP. Manganese-enhanced magnetic resonance imaging of mouse brain after systemic administration of MnCl2: dose-dependent and temporal evolution of T1 contrast. Magn Reson Med. 2005; 53(3):640–8.10.1002/mrm.20368 [PubMed: 15723400]
15. Gallez B, Demeure R, Baudelet C, Abdelouahab N, Beghein N, Jordan B, et al. Non invasive quantification of manganese deposits in the rat brain by local measurement of NMR proton T1 relaxation times. Neurotoxicology. 2001; 22(3):387–92.10.1016/S0161-813X(01)00020-1 [PubMed: 11456339]
16. Chuang KH, Koretsky AP, Sotak CH. Temporal changes in the T1 and T2 relaxation rates (DeltaR1 and DeltaR2) in the rat brain are consistent with the tissue-clearance rates of elemental manganese. Magn Reson Med. 2009; 61(6):1528–32.10.1002/mrm.21962 [PubMed: 19353652]
17. Pautler RG, Silva AC, Koretsky AP. In vivo neuronal tract tracing using manganese-enhanced magnetic resonance imaging. Magn Reson Med. 1998; 40(5):740–8. [PubMed: 9797158]
18. Morello M, Canini A, Mattioli P, Sorge RP, Alimonti A, Bocca B, et al. Sub-cellular localization of manganese in the basal ganglia of normal and manganese-treated rats An electron spectroscopy imaging and electron energy-loss spectroscopy study. Neurotoxicology. 2008; 29(1):60–72.10.1016/j.neuro.2007.09.001 [PubMed: 17936361]
19. Kalia K, Jiang W, Zheng W. Manganese accumulates primarily in nuclei of cultured brain cells. Neurotoxicology. 2008; 29(3):466–70.10.1016/j.neuro.2008.02.012 [PubMed: 18400301]
20. Vogt S. MAPS: A set of software tools for analysis and visualization of 3D X-ray fluorescence data sets. Journal de Physique IV. 2003; 104:635.
21. Glesne D, Vogt S, Maser J, Legnini D, Huberman E. Regulatory properties and cellular redistribution of zinc during macrophage differentiation of human leukemia cells. J Struct Biol. 2006; 155(1):2–11.10.1016/j.jsb.2005.09.012 [PubMed: 16495082]
22. Schramm VL, Brandt M. The manganese(II) economy of rat hepatocytes. Fed Proc. 1986; 45(12): 2817–20. [PubMed: 3770217]
23. Aschner M, Gannon M, Kimelberg HK. Manganese uptake and efflux in cultured rat astrocytes. J Neurochem. 1992; 58(2):730–5. [PubMed: 1729413]
24. Antkowiak PF, Tersey SA, Carter JD, Vandsburger MH, Nadler JL, Epstein FH, et al. Noninvasive assessment of pancreatic beta-cell function in vivo with manganese-enhanced magnetic resonance imaging. Am J Physiol Endocrinol Metab. 2009; 296(3):E573–8.10.1152/ajpendo.90336.2008 [PubMed: 19116376]
25. Maynard LS, Cotzias GC. The partition of manganese among organs and intracellular organelles of the rat. J Biol Chem. 1955; 214(1):489–95. [PubMed: 14367406]
26. Sakurai H, Nishida M, Yoshimura T, Takada J, Koyama M. Partition of divalent and total manganese in organs and subcellular organelles of MnCl2-treated rats studied by ESR and neutron activation analysis. Biochim Biophys Acta. 1985; 841(2):208–14. [PubMed: 2990573]
27. Lyden A, Larsson BS, Lindquist NG. Autoradiography of manganese: accumulation and retention in the pancreas. Acta Pharmacol Toxicol (Copenh). 1983; 52(3):205–10. [PubMed: 6405580]
28. Kodama H, Shimojo N, Suzuki KT. Distribution of manganese in rat pancreas and identification of its primary binding protein as pro-carboxypeptidase B. Biochem J. 1991; 278(Pt 3):857–62. [PubMed: 1898371]
29. Okamoto Y, Oshima R, Inagaki K, Aita S, Nisioka H, Kondo Y, et al. The presence of a manganese-rich particle in lysosome of rat pancreas due to excess manganese treatment. Biochem Mol Biol Int. 1997; 41(2):389–94. [PubMed: 9063579]
30. Rorsman P, Berggren PO, Hellman B. Manganese accumulation in pancreatic beta-cells and its stimulation by glucose. Biochem J. 1982; 202(2):435–44. [PubMed: 7046732]
31. Rorsman P, Hellman B. The interaction between manganese and calcium fluxes in pancreatic beta-cells. Biochem J. 1983; 210(2):307–14. [PubMed: 6190477]
32. Zhang N, Fitsanakis VA, Erikson KM, Aschner M, Avison MJ, Gore JC. A model for the analysis of competitive relaxation effects of manganese and iron in vivo. NMR Biomed. 2009; 22(4):391–404.10.1002/nbm.1348 [PubMed: 19137511]

33. Kwik-Uribe C, Smith DR. Temporal responses in the disruption of iron regulation by manganese. J Neurosci Res. 2006; 83(8):1601–10.10.1002/jnr.20836 [PubMed: 16568477]
34. Low W, Brawarnick N, Rahamimoff H. The inhibitory effect of Mn2+ on the ATP-dependent Ca2+ pump in rat brain synaptic plasma membrane vesicles. Biochem Pharmacol. 1991; 42(8): 1537–43. [PubMed: 1656989]
35. Twining BS, Baines SB, Fisher NS, Maser J, Vogt S, Jacobsen C, et al. Quantifying trace elements in individual aquatic protist cells with a synchrotron X-ray fluorescence microprobe. Anal Chem. 2003; 75(15):3806–16. [PubMed: 14572047]
36. Gunter TE, Gavin CE, Gunter KK. The case for manganese interaction with mitochondria. Neurotoxicology. 2009; 30(4):727–9.10.1016/j.neuro.2009.05.003 [PubMed: 19465053]
37. Gunter TE, Gavin CE, Aschner M, Gunter KK. Speciation of manganese in cells and mitochondria: a search for the proximal cause of manganese neurotoxicity. Neurotoxicology. 2006; 27(5):765–76.10.1016/j.neuro.2006.05.002 [PubMed: 16765446]
38. Kennedy SD, Bryant RG. Manganese-deoxyribonucleic acid binding modes. Nuclear magnetic relaxation dispersion results. Biophys J. 1986; 50(4):669–76. [PubMed: 3779006]
39. Wang KY, Gerena L, Swaminathan S, Bolton PH. Determination of the number and location of the manganese binding sites of DNA quadruplexes in solution by EPR and NMR. Nucleic Acids Res. 1995; 23(5):844–8. [PubMed: 7708501]
40. Polyanichko AM, Andrushchenko VV, Chikhirzhina EV, Vorob'ev VI, Wieser H. The effect of manganese(II) on DNA structure: electronic and vibrational circular dichroism studies. Nucleic Acids Res. 2004; 32(3):989–96.10.1093/nar/gkh242 [PubMed: 14872058]
41. Aschner M, Guilarte TR, Schneider JS, Zheng W. Manganese: recent advances in understanding its transport and neurotoxicity. Toxicol Appl Pharmacol. 2007; 221(2):131–47.10.1016/j.taap.2007.03.001 [PubMed: 17466353]
42. Hunter DR, Haworth RA, Berkoff HA. Cellular manganese uptake by the isolated perfused rat heart: a probe for the sarcolemma calcium channel. J Mol Cell Cardiol. 1981; 13(9):823–32. [PubMed: 6271977]
43. Fridlyand LE, Tamarina N, Philipson LH. Modeling of Ca2+ flux in pancreatic beta-cells: role of the plasma membrane and intracellular stores. Am J Physiol Endocrinol Metab. 2003; 285(1):E138–54.10.1152/ajpendo.00194.2002 [PubMed: 12644446]
44. Ainscow EK, Rutter GA. Glucose-stimulated oscillations in free cytosolic ATP concentration imaged in single islet beta-cells: evidence for a Ca2+-dependent mechanism. Diabetes. 2002; 51(Suppl 1):S162–70. [PubMed: 11815476]
45. Van Baelen K, Dode L, Vanoevelen J, Callewaert G, De Smedt H, Missiaen L, et al. The Ca2+/Mn2+ pumps in the Golgi apparatus. Biochim Biophys Acta. 2004; 1742(1-3):103–12.10.1016/j.bbamcr.2004.08.018 [PubMed: 15590060]
46. Fairclough RJ, Dode L, Vanoevelen J, Andersen JP, Missiaen L, Raeymaekers L, et al. Effect of Hailey-Hailey Disease mutations on the function of a new variant of human secretory pathway Ca2+/Mn2+-ATPase (hSPCA1). J Biol Chem. 2003; 278(27):24721–30.10.1074/jbc.M300509200 [PubMed: 12707275]
47. Mitchell KJ, Tsuboi T, Rutter GA. Role for plasma membrane-related Ca2+-ATPase-1 (ATP2C1) in pancreatic beta-cell Ca2+ homeostasis revealed by RNA silencing. Diabetes. 2004; 53(2):393–400.10.2337/diabetes.53.2.393 [PubMed: 14747290]
48. Kang YS, Gore JC, Armitage IM. Studies of factors affecting the design of NMR contrast agents: manganese in blood as a model system. Magn Reson Med. 1984; 1(3):396–409. [PubMed: 6443783]
49. Nordhoy W, Anthonsen HW, Bruvold M, Jynge P, Krane J, Brurok H. Manganese ions as intracellular contrast agents: proton relaxation and calcium interactions in rat myocardium. NMR Biomed. 2003; 16(2):82–95.10.1002/nbm.817 [PubMed: 12730949]
50. Sotak CH, Sharer K, Koretsky AP. Manganese cell labeling of murine hepatocytes using manganese(III)-transferrin. Contrast Media Mol Imaging. 2008; 3(3):95–105.10.1002/cmmi.235 [PubMed: 18546093]
51. Waghorn B, Edwards T, Yang Y, Chuang KH, Yanasak N, Hu TC. Monitoring dynamic alterations in calcium homeostasis by T (1)-weighted and T (1)-mapping cardiac manganese-enhanced MRI

in a murine myocardial infarction model. NMR Biomed. 2008; 21(10):1102–11.10.1002/nbm.1287 [PubMed: 18780285]

52. Lee LW, So PW, Price AN, Parkinson JRC, Larkman DJ, Halliday J, et al. Manganese enhancement in non-CNS organs. NMR Biomed. 2010; 23(8):931–938.10.1002/nbm.1513 [PubMed: 20878971]

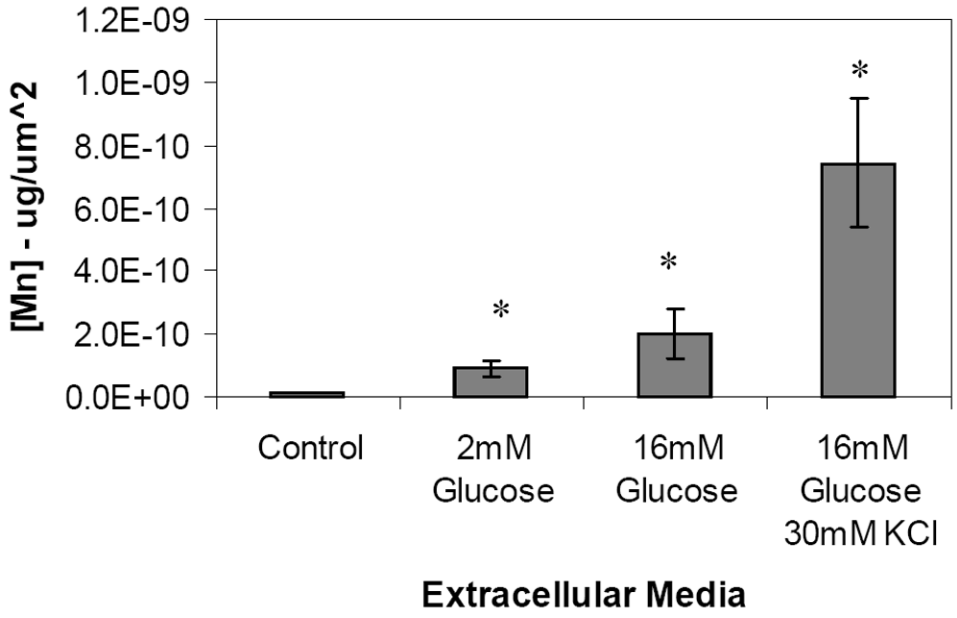

Figure 1. Quantification of intracellular manganese in MIN-6 cells

Manganese was quantified from XFM scans of fixed MIN-6 cells by selecting regions of interest corresponding to single cells. Samples were incubated for 20 minutes in KRB supplemented with a) 2mM glucose and 50 μM $MnCl_2$ (n=11) ; b) 16.7 mM glucose and 50 μM $MnCl_2$ (n=9); c) 16.7 mM glucose, 30mM KCl and 50 μM $MnCl_2$ (n=7). Cells grown in standard cell culture media were used as control (d, n=8). (mean ± SD, $p<0.001$)

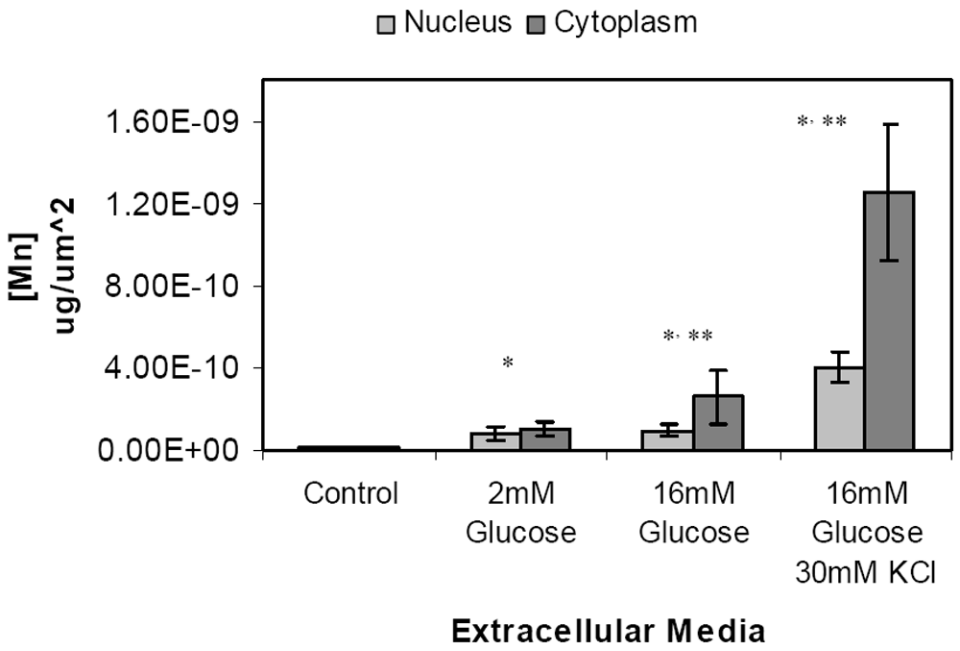

Figure 2. Manganese distribution in nucleus and cytoplasm of MIN-6 cells

Manganese concentration, expressed as $\mu g/\mu m^2$, in nucleus and cytoplasm of MIN-6 cells. Manganese was quantified from XFM scans of fixed MIN-6 cells. ROIs corresponding to single cells were traced and phosphorous rich regions within each cell corresponding to the nucleus were traced. Samples were incubated for 20 minutes in KRB supplemented with a) 2mM glucose and 50 μM $MnCl_2$ (n=11) ; b) 16.7 mM glucose and 50 μM $MnCl_2$ (n=9); c) 16.7 mM glucose, 30mM KCl and 50 μM $MnCl_2$ (n=7). Cells grown in standard cell culture media were used as control (d, n=8). (mean ± SD, $p<0.005$)

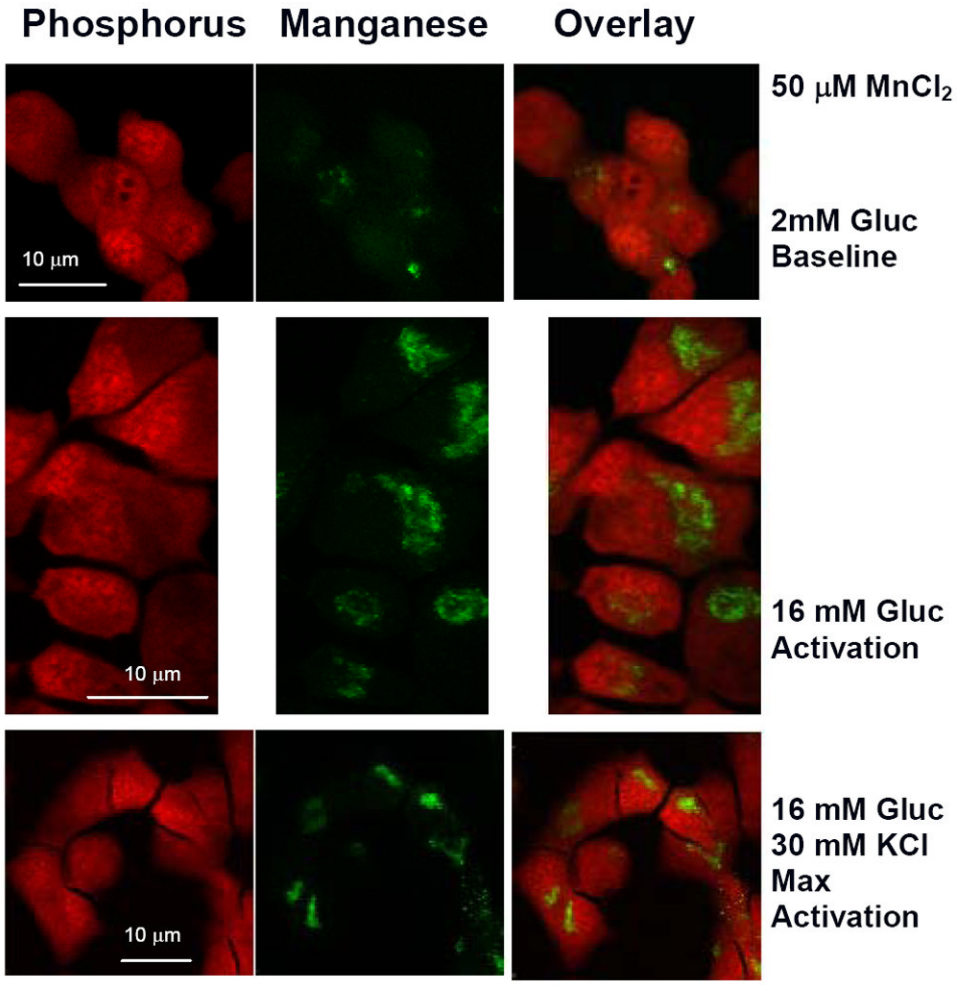

Figure 3. Visualization of manganese in XFM scans of MIN-6 cells

Representative XFM scans of MIN-6 cells. Samples were incubated for 20 minutes in KRB supplemented with 50 μM $MnCl_2$ and top row) 2mM glucose; middle row) 16.7 mM glucose; bottom row) 16.7 mM glucose and 30mM KCl. Phosphorous rich regions corresponding to cell nuclei were pseudocolored in red (left column). Manganese rich regions are represented by green pseudocoloring (middle column). Cytoplasmic localization of manganese is shown in the image overlays (right column). Color intensity is dependent on the element concentration. XFM scans were acquired with 200×200 nm resolution.

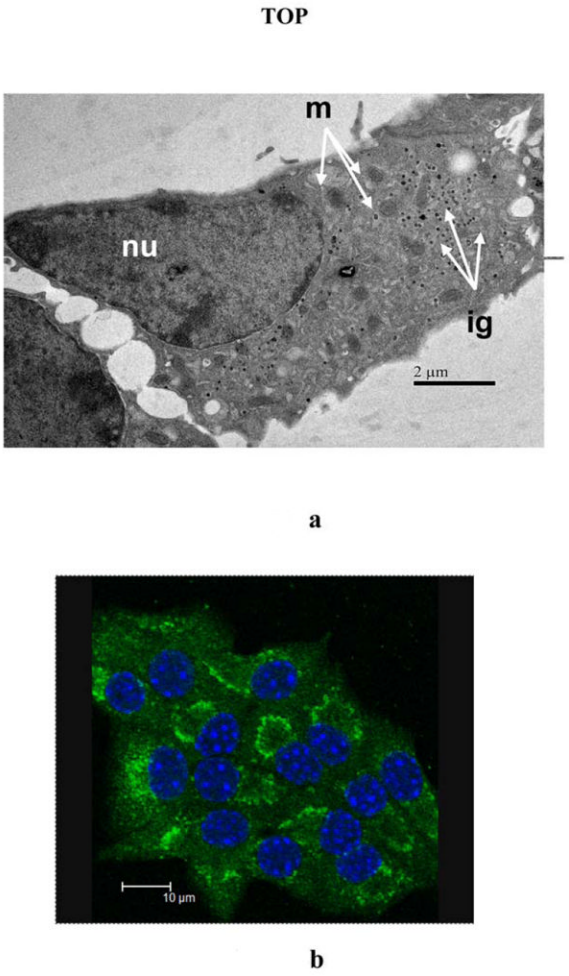

Figure 4. Representative SEM and Fluorescent staining of MIN-6 cells

a)SEM micrograph of an ultra-thin section of MIN-6 cells. MIN-6 cells incubated with 50 μM $MnCl_2$ and 2mM glucose, 16 mM glucose, or 16mM glucose and 30mM KCl were fixed with osmium tetroxide and stained with uranyl acetate. A representative cell from the 50 μM $MnCl_2$ and 16mM glucose sample is shown. Among the cellular structures clearly visible are the nucleus (nu), mitochondria (m), and insulin granules (ig). b) Fluorescent staining of Golgi apparatus in MIN-6 cells. Golgi apparatus shown as intense green areas in MIN-6 cells was stained with green-fluorescent Alexa Fluor® 488 conjugate of HPA lectin. Nuclei were counterstained with DAPI.